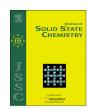
FISEVIER

Contents lists available at SciVerse ScienceDirect

# Journal of Solid State Chemistry

journal homepage: www.elsevier.com/locate/jssc



# Hydrothermal synthesis and structural analysis of new mixed oxyanion borates: $Ba_{11}B_{26}O_{44}(PO_4)_2(OH)_6$ , $Li_9BaB_{15}O_{27}(CO_3)$ and $Ba_3Si_2B_6O_{16}$



Carla Heyward, Colin D. McMillen, Joseph Kolis\*

Department of Chemistry and Center for Optical Materials Science and Engineering Technologies (COMSET), Clemson University, 485 H.L. Hunter Laboratories, Clemson, SC 29634, USA

### ARTICLE INFO

Article history:
Received 14 March 2013
Received in revised form
11 April 2013
Accepted 14 April 2013
Available online 24 April 2013

Keywords: Hydrothermal Single crystal structure Borate-phosphate Borate-carbonate Borosilicate

#### ABSTRACT

Several new borate compounds,  $Ba_{11}B_{26}O_{44}(PO_4)_2(OH)_6$  (1),  $Li_9BaB_{15}O_{27}(CO_3)$  (2), and  $Ba_3Si_2B_6O_{16}$  (3) were synthesized containing other hetero-oxyanion building blocks in addition to the borate frameworks. They were all prepared under hydrothermal conditions and characterized by single crystal and powder X-ray diffraction, and IR spectroscopy. Crystal data: For 1; space group  $P2_1/c$ , a=6.8909 (14) Å, b=13.629 (3) Å, c=25.851 (5) Å,  $\beta=90.04$  (3)°; For 2; space group P-31c, a=8.8599 (13) Å, c=15.148 (3) Å; For 3; space group P-1, a=5.0414 (10) Å, b=7.5602 (15) Å, c=8.5374 (17) Å,  $\alpha=77.15$  (3)°,  $\beta=77.84$  (3)°,  $\gamma=87.41$  (3)° for 3. Compounds 1 and 2 contain isolated oxyanions  $[PO_4]^{3-}$  and  $[CO_3]^{2-}$  respectively, sitting in channels created by the borate framework, while structure 3 has the  $[SiO_4]^{4-}$  groups directly bonded to the borate groups creating a B-O-Si framework.

© 2013 Elsevier Inc. All rights reserved.

#### 1. Introduction

In the last few decades, there has been an increase in research in metal borates as opto-electronic materials because of their excellent physical and optical properties [1–3]. Metal borates are more than twice as likely to crystallize in acentric space groups than the overall population of inorganic solids. They typically have wide transparency ranges with some having band edges as low as 147 nm. Most borates also have high optical damage thresholds and excellent thermal and chemical stability making them very promising as deep UV non-linear optical materials [1-4]. The unique structural chemistry of metal borates can be attributed to the two different coordination environments of the boron-oxygen building blocks, as they occur in both trigonal planar and tetrahedral environments. These two building blocks can occur together in various combinations, leading to a number of borate polyanions built from isolated groups, rings, chains, frameworks, sheets and many combinations thereof [4-7]. Because of these important qualities the systematic development of new borate crystals is of considerable interest.

Conventional melt-based crystal growth methods can be problematic in synthesizing metal borates due to incongruent melting as well as the typical viscous nature of the borate flux melts. This can lead to glassy products making it difficult to grow optical quality metal borate single crystals. Due to these difficulties, other synthetic methods such as hydrothermal crystal growth for these types of materials are explored. Hydrothermal crystal growth is an attractive method for making metal borate crystals because it eliminates the problems of incongruent melting and thermal strain, resulting in higher quality crystals. Since the metal borates are amphoteric like silicates and phosphates, under hydrothermal conditions, even the slightest change in reaction parameters can lead to an almost infinite number of different structures. Our group has demonstrated this by synthesizing a wide variety of new high quality single crystals over the years [8–11].

Similar to borates, other amphoteric oxyanions like phosphates, silicates, beryllates, vanadates, and carbonates have the ability to form locally acentric coordination environments with other metal ion building blocks in solids. In general the metal ions used in the lattices are empty shell species like s block ions or do transition metals. Considering the excellent properties of borates (β-BaB<sub>2</sub>O<sub>4</sub> (BBO) and LiB<sub>3</sub>O<sub>5</sub> (LBO)) and other oxyanions like phosphates and silicates, we felt that we could significantly extend the solid state phase space of borate solids if we could systematically introduce additional oxyanions into the borate lattice. It was not clear to us initially whether we could actually induce other oxyanion building blocks to incorporate into borate lattices using hydrothermal methods, but we anticipated that the combination of mixed oxyanion borates in the same crystal might generate new structures, and hopefully new NLO materials with enhanced properties. Naturally occurring minerals of borate phosphates and borate

<sup>\*</sup> Corresponding author. Fax: +864 656 6613.

E-mail addresses: cheywar@clemson.edu (C. Heyward),
cmcmill@clemson.edu (C.D. McMillen), kjoseph@clemson.edu (J. Kolis).

carbonates tend to form hydrated structures composed of borate chains forming channels with ordered [PO<sub>4</sub>]<sup>3-</sup> or [CO<sub>3</sub>]<sup>2-</sup> sites [7,12–14]. Borosilicate structures are known as natural minerals and more abundantly as glasses or ceramics made of complex layers and frameworks [7,12]. A more in-depth review of borate phosphate, borate carbonate, and borosilicate structures in the literature will be discussed in the structure analysis sections of this paper. There are a significant number of known mixed oxyanion borate minerals [7] or glasses, but the research is not as extensive in synthetic crystalline mixed oxyanion borates. Thus we wished to start to determine the scope and limitations of new oxyanion building blocks in metal borate lattices. Previously we successfully grew non-centrosymmetric structures containing berylloborates of various types including KBe<sub>2</sub>BO<sub>3</sub>F<sub>3</sub> (KBBF), Sr<sub>2</sub>Be<sub>2</sub>B<sub>2</sub>O<sub>7</sub> (SBBO), as well as other borate-beryllate structures Sr<sub>3</sub>Be<sub>2</sub>B<sub>5</sub>O<sub>12</sub>(OH) and Ba<sub>3</sub>Be<sub>2</sub>B<sub>5</sub>O<sub>12</sub>(OH) using hydrothermal growth techniques [9–11]. In this paper we describe our initial successful attempts to grow other oxyanion borates including those with phosphate, silicate, and carbonate building blocks. Herein we report the hydrothermal synthesis and structural analysis of barium containing borates mixed with oxyanions  $[PO_4]^{3-}$ ,  $[CO_3]^{2-}$ , and  $[SiO_4]^{4-}$ , namely  $Ba_{11}B_{26}O_{44}(PO_4)_2(OH)_6$ ,  $Li_9BaB_{15}O_{27}(CO_3)$ , and  $Ba_3Si_2B_6O_{16}$ . The borosilicate Ba<sub>3</sub>Si<sub>2</sub>B<sub>6</sub>O<sub>16</sub> has been previously characterized by powder X-ray diffraction but there has been no literature report of the single crystal structure. Of particular interest to us is the crystal chemical behavior of the oxyanions and whether the oxyanion species act independently as isolated units or in concert with the borate networks in building the overall structure. The reported results indicate these systems do exhibit a great variety of structural arrangements and suggest there may be a vast number of new phases available for study in these systems.

#### 2. Experimental

#### 2.1. Synthesis

Crystals of 1 were grown through a direct hydrothermal synthesis using 0.04 g (0.21 mmol) Ba(OH)<sub>2</sub>•H<sub>2</sub>O (Aldrich, 99.9%), 0.36 g (0.66 mmol) (NH<sub>4</sub>)<sub>2</sub>B<sub>10</sub>O<sub>16</sub>•8H<sub>2</sub>O (Alfa Aesar, 99.9%), 0.04 g (0.17 mmol) BaHPO<sub>4</sub> (Aldrich 97%) and 0.8 mL of aqueous mineralizer solution of 1 M NaOH. All powders were sealed in welded silver ampoules and loaded into a Tuttle cold seal autoclave (575  $^{\circ}$ C, 14.5 kpsi) for 6 days. The autoclave was cooled to room temperature and the crystalline products were washed with deionized water and air dried. This reaction produced two new phases in low yield, colorless needles of the target phase and colorless polyhedra of Ba<sub>3</sub>B<sub>12</sub>O<sub>20</sub>(OH)<sub>2</sub> which will be described in an additional paper at a later date. The majority of the product was identified as Ba<sub>3</sub>(PO<sub>4</sub>)<sub>2</sub> using powder X-ray diffraction. Single crystals of compounds 2-3 were obtained through a two-step synthetic process of a preparation of starting materials from a solid state melt, followed by hydrothermal treatment. The precursor powders were heated in platinum crucibles in air at 950 °C for 18 h using reaction formulas as follows: for Li<sub>9</sub>BaB<sub>15</sub>O<sub>27</sub>(CO<sub>3</sub>) (2), 5 g (72 mmol) B<sub>2</sub>O<sub>3</sub> ( Alfa Aesar 98%), 1.77 g (8.9 mmol) BaCO<sub>3</sub> (Strem 99%) and 0.64 g (27 mmol) LiOH (Aldrich 98+%); For  $Ba_3Si_2B_6O_{16}$  (3), 2.5 g (36 mmol)  $B_2O_3$  (Alfa Aesar 98%), 0.72 g (12 mmol) SiO<sub>2</sub> (Alfa Aesar 99.9%) and 1.84 g (12 mmol) BaO (Alfa Aesar 99.5%). The resultant polycrystalline powders were used as feedstock and in each case were loaded (0.3 g) into separate silver ampoules along with 1.2 mL of a mineralizer solution (1 M LiOH for 2 and 1 M NaOH for 3) and welded shut. The ampoules were placed in an autoclave with the remaining volume filled with water and heated for 6 days at 548 °C producing about 14 kpsi of pressure. Colorless hexagonal plates of 2 were formed in approximately 20% yield with  $LiBa_2B_{10}O_{16}(OH)_3$  forming as the major product. Crystals of **3** formed as colorless plates in approximately 80% yield.

#### 2.2. Crystal structure determination

Single crystals of each compound were selected and mounted on a Rigaku AFC8S diffractometer with a Mercury CCD area detector. The data were collected using graphite monochromated Mo  $K\alpha$  radiation ( $\lambda$ =0.71073 Å) at room temperature. The crystal structures were solved by direct methods and refined by full matrix least squares on  $F^2$  using the SHELXTL software package [15]. All non-hydrogen atoms were refined anisotropically.

The structure of **1** crystallizes in the monoclinic space group  $P2_1/c$ with unit cell parameters a = 6.8909 (14) Å, b = 13.629 (3) Å,  $c = 25.851(5) \text{ Å}, \ \beta = 90.04 \ (3)^{\circ}$ . The hydrogen atoms in compound **1** were located by calculating the bond valence of each oxygen atom and finding residual electron density around any underbonded oxygen atoms. These hydrogen atoms were refined isotropically with fixed coordinates. All other atoms were refined anisotropically, with an additional ISOR restraint being applied to atoms B5, B8, B6, B1, and B2 due to non-positive definite displacement parameters. The ISOR restraint was also applied to atoms O23, B9, B10 as a result of distorted thermal ellipsoids; no disorder was found and the data was statistically better as fully occupied atoms. Consecutive refinements resulted in  $R_1 = 0.0548$  for the observed data. The structure of **2** was determined in the trigonal space group P-31c with unit cell parameters a=8.8599 (13) Å, c=15.148 (3) Å and a final observed  $R_1$ =0.0209. All atoms in this structure were refined anisotropically. The structure of **3** solved with a final  $R_1 = 0.0269$  in the triclinic space group *P-1* with lattice parameters a = 5.0414 (10) Å, b = 7.5602 (15) Å, $c=8.5374 (17) \text{ Å}, \alpha=77.15 (3)^{\circ}, \beta=77.84 (3)^{\circ}, \gamma=87.41 (3)^{\circ}. \text{ Again, all}$ atoms were refined anisotropically. The maximum residual electron

Table 1
Crystal data and structure refinement for compounds 1–3.

	1	2	3
Empirical formula	Ba <sub>11</sub> B <sub>26</sub> O <sub>44</sub> (PO <sub>4</sub> ) <sub>2</sub> (OH) <sub>6</sub>		Ba <sub>3</sub> Si <sub>2</sub> B <sub>6</sub> O <sub>16</sub>
Formula weight	2787.79	853.96	789.06
Space group	$P2_{1}/c$ (no. 14)	P-31c (no. 163)	P-1 (no. 2)
a (Å)	6.8909 (14)	8.8599 (13)	5.0414 (10)
b (Å)	13.629 (3)		7.5602 (15)
c (Å)	25.581 (5)	15.148 (3)	8.5374 (17)
$\alpha$ (deg)			77.15 (3)
$\beta$ (deg)	90.04 (3)		77.84 (3)
$\gamma$ (deg)			87.41 (3)
$V(Å^3)$	2402.5 (8)	1029.8 (3)	310.1 (1)
Z	2	2	1
$D_{\rm calc}~({\rm Mg/m^3})$	3.854	2.754	4.225
Parameters	439	89	124
$\mu \ (\text{mm}^{-1})$	9.076	2.089	9.715
$\theta$ range (deg)	2.18-26.02	2.65-26.31	3.30-26.33
Reflections			
Collected	21,920	9201	2946
Independent	4731	702	1245
Observed $[I \ge 2\sigma(I)]$	3759	686	1137
R (int)	0.0855	0.0347	0.0228
Final $R$ (obs. data) <sup>a</sup>			
$R_1$	0.0548	0.0209	0.0269
$wR_2$	0.1290	0.0551	0.0641
Final R (all data)			
$R_1$	0.0726	0.0212	0.0300
$wR_2$	0.1402	0.0554	0.0659
Goodness of fit on F2	1.11	1.22	1.16
Largest diff. peak (e/ ų)	2.98	0.33	2.36
Largest diff. hole (e/ ų)	-2.10	-0.56	-1.56

<sup>&</sup>lt;sup>a</sup>  $R_1 = [\sum ||F_0| - |F_c||]/\sum |F_0|$ ;  $wR_2 = \{[\sum w[(F_0)^2 - (F_c)^2]^2]\}^{1/2}$ .

## Download English Version:

# https://daneshyari.com/en/article/7760224

Download Persian Version:

https://daneshyari.com/article/7760224

<u>Daneshyari.com</u>